Available online at www.sciencedirect.com
SCIENCE DIRECT
Surface Science 600 (2006) 716–723
SURFACE SCIENCE
www.elsevier.com/locate/susc

Chemical fingerprinting at the atomic level with scanning tunneling spectroscopy

Koji S. Nakayama [a,b,*], Tomoko Sugano [a,1], Kenji Ohmori [b,2], A.W. Signor [a], J.H. Weaver [a,b]

[a] Department of Materials Science and Engineering, University of Illinois at Urbana-Champaign, Urbana, IL 61801, USA
[b] Frederick Seitz Materials Research Laboratory, University of Illinois at Urbana-Champaign, Urbana, IL 61801, USA

Received 28 March 2005; accepted for publication 29 November 2005
Available online 29 December 2005

Abstract

Scanning tunneling spectroscopy (STS) based on scanning tunneling microscopy (STM) makes it possible to map the local electronic density of states for clean surfaces and for those with adsorbates. We have developed a protocol that allows us to obtain the spectral fingerprints of halogen atoms on Si(001), and we use those fingerprints to distinguish between adatom species for surfaces with Cl and Br mixed adsorbates. The key to the process is the energy distribution of the antibonding states that depend on the halogen species.

Keywords: Scanning tunneling spectroscopy; Local density of states; Si(001) with adsorbed halogens; Chemical identification

1. Introduction

Atomic-scale chemical analysis has been a long-standing goal of materials characterization. It requires the ability to interrogate individual atoms and to recognize their distinguishing signatures. Scanning tunneling microscopy (STM) offers the needed spatial resolution and sensitivity, and it has been used with great success to determine the atomic structure of clean surfaces and surfaces with steps, defects, and adsorbates. Scanning tunneling spectroscopy (STS) offers insights into the electronic properties of those surfaces and adsorbates [1]. An early example of spectroscopy involved voltage-dependent imaging of GaAs(110) where dual bias imaging was needed to distinguish the Ga and As sublattices [2]. Recently, STS studies have tended to focus on the local electronic properties, such as Cu on Mo(110) [3], Fe on Au(100) [4], B dopants on Si(111) [5], and B on hydrogen-terminated Si(001) [6,7]. Another very recent study compares spectra collected at different Al adsorption sites on GaAs(001) and couples this with density functional theory calculations [8]. In these studies, STS spectra were collected at individual adsorption sites to examine the electronic states.

In this paper, extend STS examinations to map the electronic states as a function of energy and position across the surface [9]. In this way, we show that the energy distribution of the electronic states makes chemical recognition possible for halogen adatoms on Si(001). To demonstrate this, we measured current–voltage spectra throughout the scanned area to obtain three-dimensional maps of the local density of states (LDOS). We exploit the fact that the energy levels depend on the adatom species and the substrate,

* Corresponding author. Address: Institute for Materials Research, Tohoku University, 2-1-1, Katahira, Aoba-ku, Sendai 980-8577, Japan. Tel.: +81 222152582; fax: +81 222152381.
E-mail address: kojisn@imr.tohoku.ac.jp (K.S. Nakayama).
[1] Permanent address: Japan Patent Office, Kasumigaseki, Tokyo 100-8915, Japan.
[2] Current address: National Institute for Materials Science, Nano Materials Laboratory, Ibaraki 305-0044, Japan.

0039-6028/$ - see front matter © 2005 Elsevier B.V. All rights reserved.
doi:10.1016/j.susc.2005.11.032

and we show that chlorine can be distinguished from chemically similar bromine through its state distribution. We further generalize that iodine could be distinguished from Cl and Br, based on comparison of antibonding energy levels. The protocol developed here, with its emphasis on the distribution and distinction of energy states, should be applicable to other systems, and should yield new insights regarding chemical identification.

2. Experimental considerations

The experiments were performed in an ultrahigh vacuum system with a base pressure of 4×10^{-11} Torr. The samples were p-type Si wafers (B-doped, 0.01 Ω cm, Virginia Semiconductor Inc.) that were oriented within 0.5° of (0 0 1). Clean Si(0 0 1) surfaces were prepared by thermal cleaning in ways that kept the initial defect density below ~1% [10]. We used solid state electrochemical cells based on AgX doped with CdX_2 (~5% weight ratio), where X = Cl, Br, or I [11]. After characterization with STM topographs, the surfaces were exposed at room temperature to a flux of halogens [12–15]. For X-Si(0 0 1)-(2 × 1), there is one halogen for each surface Si atom and such chemisorption preserves the 2 × 1 reconstruction associated with Si atom dimerization.

We used an Omicron Nanotechnology STM operating at 80 K for topographic imaging and tunneling spectroscopy. For the latter, we used current imaging tunneling spectroscopy (CITS) [9,16] whereby the tunneling current–voltage (I–V) curves were recorded at each pixel of a scanned area while the tunneling gap was fixed by momentarily turning off the feedback loop. We scanned 200 × 200 pixels for current imaging (400 × 400 pixels for STM). A CITS image represents one slice of the three-dimensional STS database of $I(V,x,y)$ at a given sample bias. Current maps can be constructed from a section of $I(V,x,y)$ for any bias, and variations reflect changes in the electronic states accessed. To map the local density of states of the surface, we numerically calculated the normalized tunneling conductance, $[(\mathrm{d}I/\mathrm{d}V)/(I/V)]$, which is taken to be independent of the transmission factor [17,18]. To avoid divergence at $V = 0$ in the conductance calculation, we added a current of $\Delta I = 6 \times 10^{-4}$ nA which is equivalent to the noise level of the current detection. LDOS maps

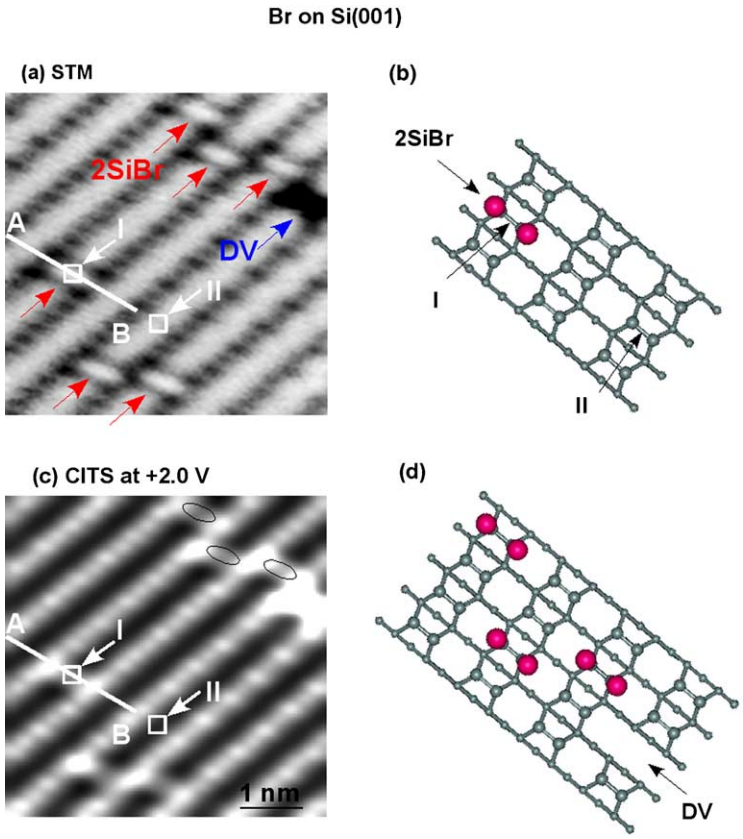

Fig. 1. Topographic and spectroscopic features of Br on Si(0 0 1). (a) A topograph acquired at 80 K (tunneling current 0.5 nA, sample bias −2.0 V, scan area 5 × 5 nm^2). The dimer rows run diagonally, and static dimers can be recognized in the upper left and lower right corners of the image. The ball-and-stick model of (b) shows two Br adatoms bonded to a Si dimer, labelled 2SiBr. Site I is located over the center of the 2SiBr unit while site II is over a Br-free dimer. (c) A CITS image where the I–V behavior was measured at each pixel with the tip at a fixed height (set at −2.0 V with tunneling current 0.5 nA). The current was derived from electrons tunneling into empty states within +2.0 V of the Fermi level. (d) A model of the complex of three 2SiBr units and one DV identified in (a) and (c).

were then constructed from sections of $[(dI/dV)/(I/V)](V,x,y)$ at given energies (sample biases).

The STM tips were produced from tungsten wires (0.38 mm diameter) that were electrochemically etched by KOH and cleaned by electron bombardment in ultrahigh vacuum. The experiments were carried out several times with different tips. Repeated scanning of the same area with electrons tunneling from tip to sample verified that there were no structural changes in the surface involving adatom desorption stimulated by tunneling electron irradiation or movement of adsorbates.

3. Topographic and tunneling current images

Fig. 1(a) is an STM topograph of Si(0 0 1) with a Br concentration of ~0.03 monolayer (ML). The image was obtained with electrons tunneling (current 0.5 nA) to the tip from the sample (biased at −2.0 V). The bright Si-dimer rows run diagonally across the image. Chemisorption is dissociative, and the halogen adatoms bond to dangling bonds of the Si dimers. Pairwise bonding with two halogens on a single dimer is energetically favored [19], and mild heating (~650 K) promotes such bonding. In Fig. 1(a), 12 Br adatoms are pairwise bonded to six Si dimers, red[3] arrows, and there is a dark dimer vacancy, DV. Fig. 1(b) illustrates a pair of Br adatoms on one dimer, labelled 2SiBr. A small area with c(4 × 2) symmetry can be recognized in the lower right corner of Fig. 1(a). Br-free dimers around 2SiBr units appear as ovals, indicating their dynamic motion at 80 K. Such destabilization of the c(4 × 2) reconstruction is consistent with a recent demonstration by Chen and Boland [20] that hydrogen chemisorption introduces strain that reduces the barrier for buckling on dimers near adsorbates.

The spectroscopic image of Fig. 1(c) represents a slice of the $I(V,x,y)$ STS database for the same area as (a). It was constructed from 200 × 200 pixels for the 5 × 5 nm^2 area. The image represents an atomic-resolution map of the tunneling current for electrons tunneling into states 2.0 eV above the Fermi level. Two boxes labelled I and II are defined in Fig. 1(a)–(c) and line AB crosses a 2SiBr unit. The conductance (current) of the 2SiBr unit (position I) is higher than that at the center of a Br-free dimer (position II). The troughs between dimer rows have intermediate currents. The highest conductance in the image was associated with the dimer vacancy. Three 2SiBr sites appear near the DV, and the adsorbate distribution for them is depicted in Fig. 1(d). The lower two in the image are on adjacent rows, offset by one dimer. This offset is common for bromine [21–23] and iodine [14,15] at intermediate coverage since the c(4 × 2) pattern is favored. Moreover, the end of the high conduction region of the DV intersects the region of the 2SiBr unit, implying a rearrangement of states [better seen in Fig. 3(a)].

[3] For interpretation of colours in Figs. 1, 3, 4 and 5, the reader is referred to the web version of this article.

4. Tunneling characteristics of adsorption sites

Fig. 2(a) shows I–V curves that were obtained from squares I and II in Fig. 1. Each spectrum was averaged over groups of 10 × 10 pixels. The peaks near 0 V are electrical noise, and they are below 5×10^{-4} nA. The current at position I increases rapidly as Si–Br antibonding σ* states are accessed [13,24] and the current at those sites was ~3 times that of a Br-free dimer at +3 V.

The I–V curves in Fig. 2(a) (also the CITS image of Fig. 1(c)) contains both geometric and electronic information because the tunneling current can be derived from the energy integral of the product of the local density of states and the transmission probability, where the latter involves a factor of tip–sample separation. To obtain the LDOS component, we numerically calculated, site-by-site, the normalized differential conductance, $[(dI/dV)/(I/V)]$, which removes the transmission factor [17,18].

Fig. 2(b) shows $(dI/dV)/(I/V)$ spectra taken along line AB. Curve I shows a broad structure at negative bias around −1.7 V. Lee and Kang [24] reported the results of first principles calculations for Br- and Cl-saturated Si(0 0 1) that showed Si–Br and Si–Cl bonding states around −4 eV, too deep to be observed in our experiments. We associate the peak with energy lower than −1.7 eV in Fig. 2(b) with Si σ states that are slightly modified due to Br adsorption. The prominent feature around −0.5 eV reflects tunneling from occupied π states near the valence band maximum, and the feature at 0.8 eV reflects tunneling into empty π* states, as identified previously by many groups [25–35]. The feature around 1.4 eV also arises from π* states, as discussed in detail elsewhere [36]. To demonstrate that these features are indeed surface derived, we saturated the surface with Br and performed spectroscopic measurements at 80 K. Fig. 2(c) shows I–V and $(dI/dV)/(I/V)$ spectra taken from the center of a 2SiBr site, equivalent to site I in Fig. 1(a). The gap expands to ~1.7 eV and the contributions attributed to π and π* states were quenched in the $(dI/dV)/(I/V)$ spectrum, as they should be. The Si–Br σ* states have broadened into a manifold that starts at ~1.4 eV.

The difference curve shown at the bottom of Fig. 2(b) was obtained by subtracting curve II from I to emphasize changes induced by Br adsorption. The effect is profound in the region of the higher π* states, and the feature at ~2 eV is a manifestation of the Si–Br σ* levels. The difference curve shows the extent of the states at 1.4 eV and above 2.0 eV. Following Yokoyama et al. [30], the enhanced intensity at 1.4 eV over a 2SiBr site is consistent with the halogen sites acting as potential energy barriers that confine or scatter π* states that propagate along the dimer rows (but not across rows).

Fig. 2(d) shows spectra measured at equivalent positions relative to a 2SiCl unit for dilute amounts of Cl on Si(1 0 0).

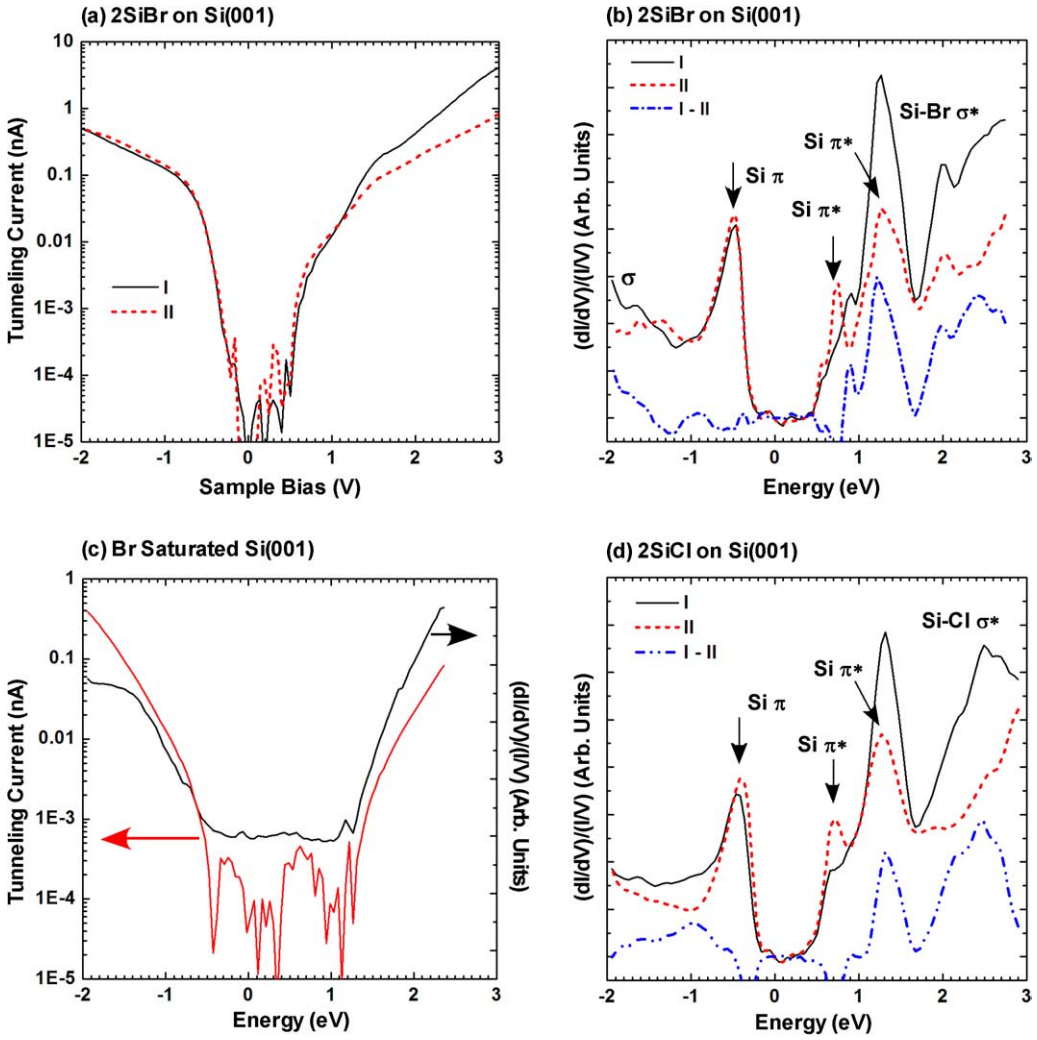

Fig. 2. *I–V* and LDOS spectra on halogen covered Si(001)-c(4 × 2). (a) *I–V* spectra taken in squares I and II along line *AB* defined in Fig. 1. (b) $(dI/dV)/(I/V)$ spectra taken in those same places. The bottom-most curve represents the difference between I and II to emphasize the effect of Br adsorption. (c) *I–V* curve and $(dI/dV)/(I/V)$ spectrum at 80 K taken from Br saturated Si(001) at positions equivalent to I. The current is scaled logarithmically (right) and $(dI/dV)/(I/V)$ spectrum is scaled by arbitrary units (left). (d) Analogous spectra obtained for dilute amounts of Cl on Si(001).

Again, the difference curve indicates Si–Cl states centered around 2.4 eV. From chemical bonding arguments, it is also reasonable that the σ–σ^* splitting would be smaller for Br than for Cl and the Si–Br σ^* states would be lower than the Si–Cl σ^* states, as revealed in Fig. 2(b) and (d).

5. Local density of states of halogen adsorbates

Fig. 3 shows the same area as Fig. 1(a) and (c) constructed from the normalized differential conductance at energies that correspond to the maxima in $[(dI/dV)/(I/V)]$ spectra of Fig. 2(b). The effect of Br adsorption is particularly evident in the LDOS map at 2.0 eV because of significantly increased conductance at the 2SiBr sites. In contrast to the current image of Fig. 1(c) where the conductance at Br-free dimers is low, the lowest LDOS is in the trough (between dimer rows), and the dimer rows themselves have intermediate LDOS intensity. The LDOS map also shows enhanced state densities associated with 2SiBr pairs and the DV. The LDOS features at 1.4 eV are more complicated; they are very different from those at 2.0 eV because the conductance is high in the trough and there are red (bright) spots along the trough. These spots arise from π^* antibonding states, as discussed elsewhere [36]. There is also strong intensity over the 2SiBr sites.

Compared with the richness of features in the empty state spectra, the images of the bonding states have relatively little spatial variation. Fig. 3(c) is the LDOS image obtained at −0.4 eV which corresponds to the π surface states. It shows the lowest (blue) conductance above 2SiBr sites. It is intriguing that the low state density region also appears around the DV. This is consistent with the report by Brown et al. [37,38] of positively charged features around vacancies. They observed a depression with a diameter of ~5 nm around a DV when p-type Si(100)-(2 × 1) was scanned with sample bias between −0.6 and −0.8 V. Fig. 3(d) shows the LDOS map at −1.7 eV. The overall intensity was low at this energy window. The Br adsorption

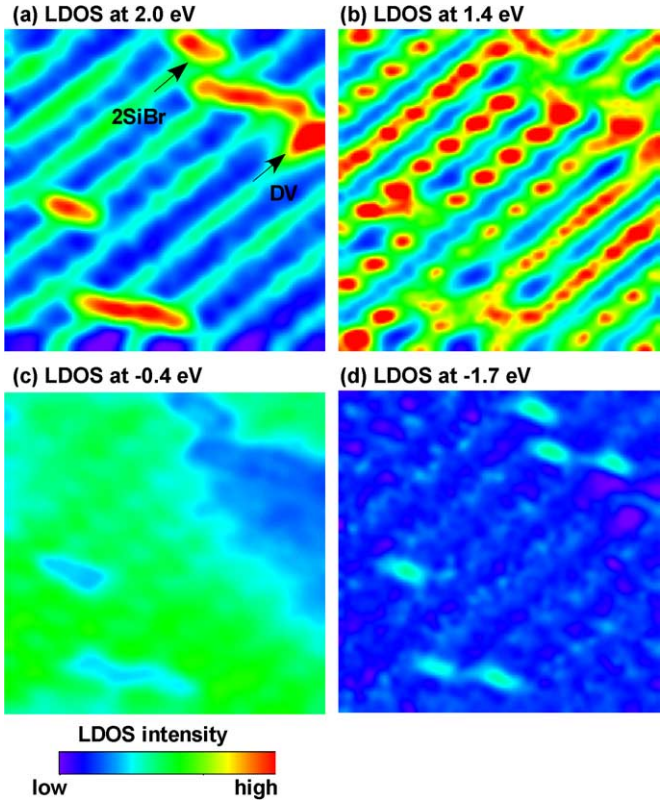

Fig. 3. LDOS images of Br on Si(001). The images have $(dI/dV)/(I/V)$ contrast and are constructed at representative energies. The effect of Br adsorption is evident at 2.0 eV, and the largest conductance (bright red) occurs at the dimer vacancy. The Si antibonding states become more evident at 1.4 eV. The energy states probed at −0.4 eV correspond to π surface states and the 2SiBr sites have the weakest intensity. At −1.7 eV, the 2SiBr sites are evident, indicating that Si states at that energy are modified by Br adsorption.

sites modify back bonds of Si and they are distinguishable against the flat background. The modification of the electronic states around −1.7 eV is different between halogens (discussed below).

6. Three-dimensional maps of the LDOS and chemical recognition

Fig. 4 shows a spatially resolved LDOS maps of Si(001)-c(4 × 2) with and without Br, Cl, or I, each constructed from 35 spectra, all averaged over 5 × 5 pixels. The spectra were taken along a line equivalent to *AB* in Fig. 1. The Si surface bandgap is reflected by the deep blue channel separating the π and π* surface states. The Fermi energy lies near the valence band maximum for these boron-doped samples. In Fig. 4(a), there are intensity fluctuations associated with the π* states around 0.8 eV, but the intensity variations associated with the π states at −0.4 eV are smaller. The intensity variations at 1.4 eV are very high, with the largest conductance in the trough and smallest over a dimer.

The effects of Cl, Br, and I adsorption are evident in Fig. 4(b)–(d). In all cases, the center position along *AB*, corresponding to the 2Si-halogen unit, is now bright at 1.4 eV. More significant is the appearance of high conductance areas over the 2SiI unit at 1.9 eV, the 2SiBr unit at 2.0 eV, and the 2SiCl unit at 2.4 eV. These then represent the halogen chemisorption signatures in a way that is more graphic than in the LDOS spectra of Fig. 2(b) and (c). The Si σ states can be recognized for the clean surface in Fig. 4(a) below −1.5 eV. Those states are modified by chemisorptions. The differences between the spectra reflect

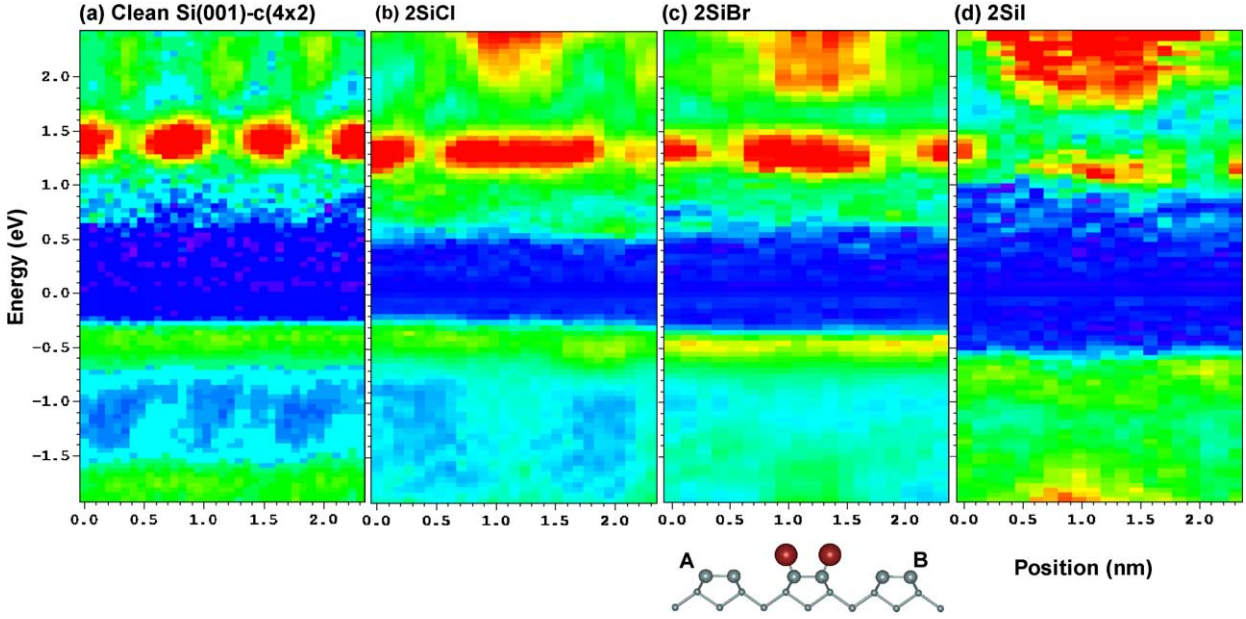

Fig. 4. Energetically and spatially resolved LDOS features of clean and halogen-adsorbed Si(001) along lines like *AB* of Fig. 1. (a) A LDOS map of the clean Si(001) surface where the gap between the π and π* surface states is ~0.8 eV (dark blue central region). The largest conductance (bright red) occurs when the tip is over the trough at 1.4 eV and it is smallest over the dimer. (b)–(d) High conductance of the 2Si-halogen dimers at 1.4 and ~2.0 eV, concentrated midway along *AB*, as depicted by the ball-and-stick model. These maps constitute the fingerprints of halogens on clean S(001).

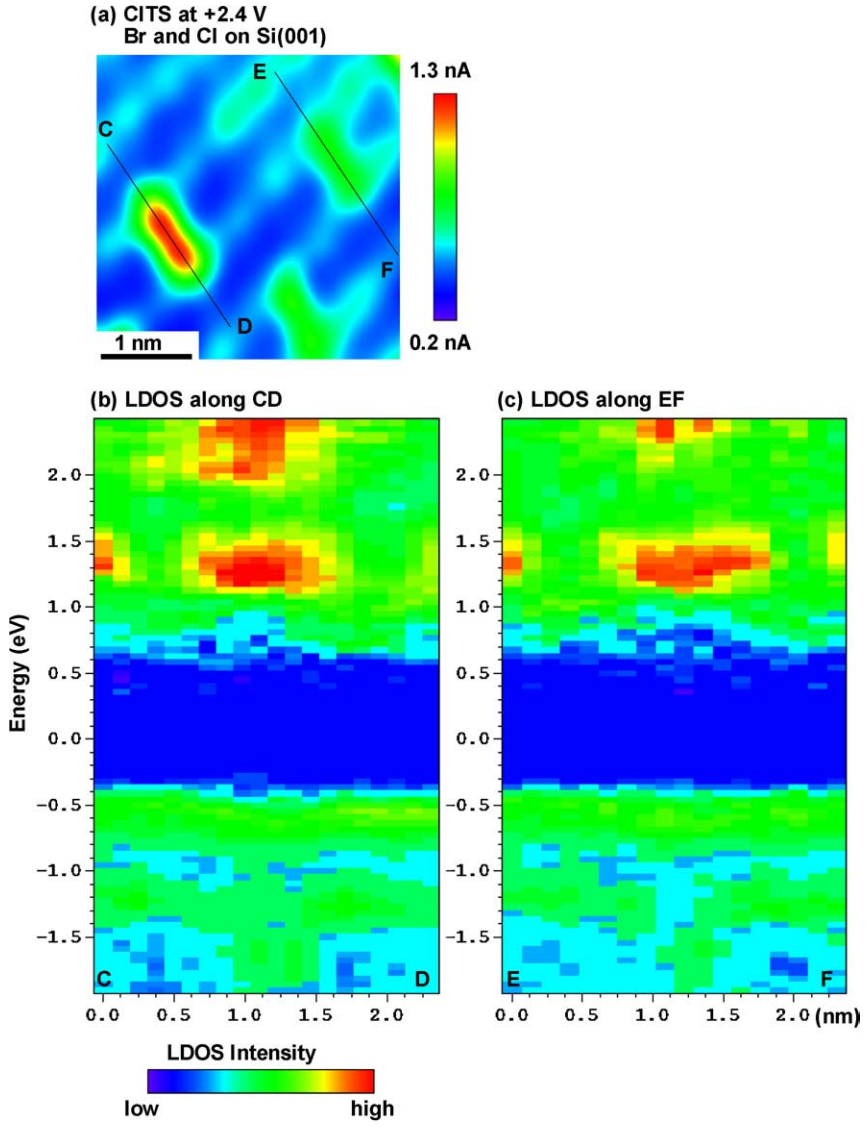

Fig. 5. CITS image and LDOS map for a surface with both 2SiBr and 2SiCl units. The image in (a) was constructed at +2.4 V. The tip position was fixed with a current of 0.5 nA at −2.0 V (scan area 3.8×3.8 nm^2). The dimer crossed by CD has high conductance and the dimer crossed by EF has intermediate intensity. (b, c) LDOS maps along CD and EF showing that the states around 2.0 eV are more apparent for CD than EF. Hence, CD crosses a 2SiBr unit and the EF crosses a 2SiCl unit.

the differences in electronegativity and extent of charge transfer from Si to the adsorbates (Si–I < Si–Br < Si–Cl). The broad and intense (red) features of antibonding states reflect the relative sizes of the adsorbates.

To test whether the LDOS differences evident in Fig. 4 would make it possible to distinguish them on a surface where both Br and Cl were present, we exposed a sample at room temperature to a flux of Br_2 and Cl_2 to accumulate a total adatom concentration of ~0.06 ML. The sample was then imaged with STM/STS. Fig. 5(a) shows a CITS image constructed at +2.4 V. Three dimers are evident but the left-most has the greatest conductance. Lines CD and EF are equivalent to *AB* in Fig. 1, centered on the Si-halogen unit. The blue lines that run diagonally correspond to the dimer rows. The trough (blue–green) has slightly higher conductance than the dimer (blue) in this current image constructed at +2.4 V. The LDOS map along line CD shown in Fig. 5(b) agrees well with Fig. 4(b) for Br on Si(0 0 1). In particular, the onset of antibonding states starts around 1.8 eV and they are strong at 2.0 eV. There is also a peak at 1.4 eV, but it is present for both Cl and Br. Fig. 5(c) shows the LDOS along line EF where the peak (red area) has been shifted at 2.4 eV, as for Cl. We conclude that line CD crosses a 2SiBr unit and that EF identifies a 2SiCl unit.

From these results, one would expect both Cl and Br to be visible at 2.4 eV in a LDOS image but that Cl would not be visible at biases below the onset of the Si–Cl LDOS feature. For a surface with mixed halogens, Fig. 6(a) confirms that all are visible at 2.4 eV but Fig. 6(b) shows that only

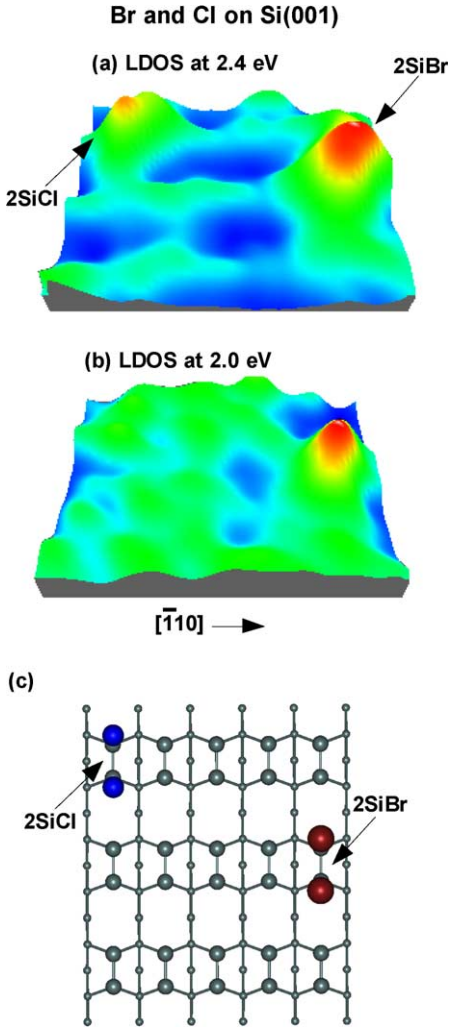

Fig. 6. LDOS images shown in perspective for a surface with both Br and Cl adatoms with the dimer row direction indicated by [$\bar{1}$ 1 0]. (a) Obtained at 2.4 eV, and both 2SiCl and 2SiBr units are visible. (b) Obtained at 2.0 eV, below the Si–Cl antibonding states but above the onset of the Si–Br states. Only the 2SiBr unit is bright. (c) Depicts the 2SiCl and 2SiBr position configurations.

one of the two sites is evident at 2 eV. We conclude that STS analysis offers chemical identification at the atomic level.

7. Conclusions

In this paper, we have developed the protocol whereby the chemical fingerprints of individual adatoms on the Si(0 0 1) surface can be acquired. What is needed is a detailed LDOS map of the clean surface so that the energy distribution of the orbitals involved in chemisorption can be quantified. This process should be widely applicable for clean surfaces with dilute amounts of adsorbates. An exciting extension of the process will focus on the transition to higher concentrations of adatoms where it should be possible to follow the onset of orbital delocalization as surface levels broaden into band states. It should be clear that STM/STS provides a remarkable tool for chemical recognition and electronic property measurement in the tunneling junction at the single atom level.

Acknowledgments

This work was supported in part by the National Science Foundation. K.O. was supported by the Department of Energy under Award No. DEFG02-91ER45439 through the Frederick Seitz Materials Research Laboratory. T.S. acknowledges support from a Japan Patent Office Fellowship.

References

[1] T.A. Jung, F.J. Himpsel, R.R. Schlittler, J.K. Gimzewski, in: K. von Klitzing, R. Wiesendanger (Eds.), Chemical Information from Scanning Probe Microscopy and Spectroscopy, Springer-Verlag, Berlin, Heidelberg, New York, 1998, p. 11, and references therein.
[2] R.M. Feenstra, J.A. Stroscio, J. Tersoff, A.P. Fein, Phys. Rev. Lett. 58 (1987) 1192.
[3] T. Jung, Y.W. Mo, F.J. Himpsel, Phys. Rev. Lett. 74 (1995) 1641.
[4] Y. Kuk, P.J. Silverman, J. Vac. Sci. Technol. A 8 (1990) 289.
[5] I.-W. Lyo, E. Kaxiras, Ph. Avouris, Phys. Rev. Lett. 63 (1989) 1261.
[6] L. Liu, J. Yu, J.W. Lyding, Appl. Phys. Lett. 78 (2001) 386.
[7] Y. Suwa, S. Matsuura, M. Fujimori, S. Heike, T. Onogi, H. Kajiyama, T. Hitosugi, K. Kitazawa, T. Uda, T. Hashizume, Phys. Rev. Lett. 90 (2003) 156101.
[8] M.J. Hale, D.L. Winn, T.J. Grassman, A.C. Kummel, J. Chem. Phys. 122 (2005) 124702.
[9] A.W. Munz, Ch. Ziegler, W. Göpel, Phys. Rev. Lett. 74 (1995) 2244.
[10] K.S. Nakayama, J.H. Weaver, Surf. Sci. 574 (2005) 331.
[11] N.D. Spencer, P.J. Goddard, P.W. Davies, M. Kitson, R.M. Lambert, J. Vac. Sci. Technol. A 1 (1983) 1554.
[12] K.S. Nakayama, E. Graugnard, J.H. Weaver, Phys. Rev. Lett. 88 (2002) 125508.
[13] K.S. Nakayama, E. Graugnard, J.H. Weaver, Phys. Rev. Lett. 89 (2002) 266106.
[14] D. Rioux, F. Stepniak, R.J. Pechman, J.H. Weaver, Phys. Rev. B 51 (1995) 10981.
[15] G.J. Xu, A.W. Signor, A. Agrawal, K.S. Nakayama, B.R. Trenhaile, J.H. Weaver, Surf. Sci. 577 (2005) 77.
[16] R.J. Hamers, R.M. Tromp, J.E. Demuth, Phys. Rev. Lett. 56 (1986) 1972.
[17] R.M. Feenstra, J.A. Stroscio, A.P. Fein, Surf. Sci. 181 (1987) 295.
[18] R.M. Feenstra, Phys. Rev. B 60 (1999) 4478.
[19] G.A. de Wijs, A. De Vita, A. Selloni, Phys. Rev. Lett. 78 (1997) 4877.
[20] D. Chen, J.J. Boland, Phys. Rev. B 65 (2002) 165336.
[21] K. Nakayama, C.M. Aldao, J.H. Weaver, Phys. Rev. B 59 (1999) 15983.
[22] C.F. Herrmann, J.J. Boland, Surf. Sci. 460 (2000) 223.
[23] G.J. Xu, E. Graugnard, B.R. Trenhaile, K.S. Nakayama, J.H. Weaver, Phys. Rev. B 68 (2003) 075301.
[24] J.Y. Lee, M.-H. Kang, Phys. Rev. B 69 (2004) 113307.
[25] P. Krüger, A. Mazur, J. Pollmann, G. Wolfgarten, Phys. Rev. Lett. 57 (1986) 1468.
[26] R.J. Hamers, Ph. Avouris, F. Bozso, Phys. Rev. Lett. 59 (1987) 2071.
[27] H. Kageshima, M. Tsukada, Phys. Rev. B 46 (1992) 6928.
[28] J.E. Northrup, Phys. Rev. B 47 (1993) 10032.
[29] H. Ikegaki, K. Ohmori, H. Ikeda, H. Iwano, S. Zaima, Y. Yasuda, Jpn. J. Appl. Phys. 35 (1996) 1593.
[30] T. Yokoyama, M. Okamoto, K. Takayanagi, Phys. Rev. Lett. 81 (1998) 3423.
[31] X.R. Qin, M.G. Lagally, Phys. Rev. B 59 (1999) 7293.

[32] K. Hata, Y. Shibata, H. Shigekawa, Phys. Rev. B 64 (2001) 235310.
[33] H. Okada, Y. Fujimoto, K. Endo, K. Hirose, Y. Mori, Phys. Rev. B 63 (2001) 195324.
[34] W. Kaminski, L. Jurczyszyn, Surf. Sci. 566–568 (2004) 29.
[35] L. Perdigao, D. Deresmes, B. Grandidier, M. Dubois, C. Delerue, G. Allan, D. Stievenard, Phys. Rev. Lett. 92 (2004) 216101.
[36] K.S. Nakayama, M.M.G. Alemany, T. Sugano, K. Ohmori, J.R. Chelikowsky, J.H. Weaver, Phys. Rev. B, in press.
[37] G.W. Brown, H. Grube, M.E. Hawley, S.R. Schofield, N.J. Curson, M.Y. Simmons, R.G. Clark, J. Vac. Sci. Technol. A 21 (2003) 1506.
[38] G.W. Brown, H. Grube, M.E. Hawley, Phys. Rev. B 70 (2004) 121301R.